The protective role of liver X receptor (LXR) during fumonisin B1-induced hepatotoxicity

Marion Régnier, Arnaud Polizzi, Céline Lukowicz, Sarra Smati, Frédéric Lasserre, Yannick Lippi, Claire Naylies, Joëlle Laffitte, Colette Bétoulières, Alexandra Montagner, et al.

Title: The protective role of liver X receptor (LXR) during fumonisin B1-induced hepatotoxicity

Authors: Marion Régnier[1], Arnaud Polizzi[1], Céline Lukowicz[1], Sarra Smati[1,2], Frédéric Lasserre[1], Yannick Lippi[1], Claire Naylies[1], Joelle Laffitte[1], Colette Bétoulières[1], Alexandra Montagner[1], Simon Ducheix[1], Pascal Gourbeyre[1], Sandrine Ellero-Simatos[1], Sandrine Menard[1], Justine Bertrand-Michel[3], Talal Al Saati[5], Jean-Marc Lobaccaro[4], Hester M. Burger[6], Wentzel C. Gelderblom [6,7], Hervé Guillou[1], Isabelle P. Oswald[#1], Nicolas Loiseau[#1]

1 Toxalim (Research Centre in Food Toxicology), Université de Toulouse, INRA, ENVT, INP-Purpan, UPS, Toulouse, France.

2 I2MC, Institut National de la Santé et de la Recherche Médicale (INSERM)-U 1048, Université de Toulouse 3 and CHU de Toulouse, Toulouse, France.

3 MetaToul-Lipidomic Facility-MetaboHUB, INSERM UMR1048, Institute of Cardiovascular and Metabolic Diseases, Université Paul Sabatier-Toulouse III, Toulouse, France.

4 Université de Clermont Auvergne, CNRS, INSERM, GReD, Clermont-Ferrand, F-63001, France.

5 INSERM/UPS/ENVT, US006/CREFRE, Histopathology Facility, Place du Docteur Baylac, CHU Purpan, Toulouse, France

6 Institute of Biomedical and Microbial Biotechnology, Cape Peninsula University of Technology, Bellville, South Africa;

7 Department of Biochemistry, University of Stellenbosch, Matieland, South Africa

[#] Correspondence and requests for materials should be addressed either to Isabelle P. OSWALD or Nicolas LOISEAU

Dr. Isabelle P. Oswald, PhD

Toxalim UMR1331 INRA/ENVT/INP/UPS

180, Chemin de Tournefeuille, BP93173, 31027 Toulouse cedex 3 – France

Tel: +33 (0)5 82 06 63 66 ; Fax: +33 (0)5 61 28 52 44

Email: isabelle.oswald@inra.fr

Dr. Nicolas Loiseau, PhD

Toxalim UMR1331 INRA/ENVT/INP/UPS

180, Chemin de Tournefeuille, BP93173, 31027 Toulouse cedex 3 – France

Tel: +33 (0)5 82 06 63 03 ; Fax: +33 (0)5 61 28 52 44

Email: nicolas.loiseau@inra.fr

Abbreviations:

Keywords

Fumonisin, Ceramide, Liver, LXR, Hepatotoxicity

ABSTRACT

Fumonisin B1 (FB1), a congener of fumonisins produced by *Fusarium* species, is the most abundant and most toxicologically active fumonisin. FB1 causes severe mycotoxicosis in animals, including nephrotoxicity, hepatotoxicity, and disruption of the intestinal barrier. However, mechanisms associated with FB1 toxicity are still unclear. Preliminary studies have highlighted the role of liver X receptors (LXRs) during FB1 exposure. LXRs belong to the nuclear receptor family and control the expression of genes involved in cholesterol and lipid homeostasis. In this context, the toxicity of FB1 was compared in female wild-type ($LXR^{+/+}$) and $LXR_{\alpha,\beta}$ double knockout ($LXR^{-/-}$) mice in the absence or presence of FB1 (10 mg/kg body weight/day) for 28 days. Exposure to FB1 supplemented in the mice's drinking water resulted in more pronounced hepatotoxicity in $LXR^{-/-}$ mice compared to $LXR^{+/+}$ mice, as indicated by hepatic transaminase levels (ALT, AST) and hepatic inflammatory and fibrotic lesions. Next, the effect of FB1 exposure on the liver transcriptome was investigated. FB1 exposure led to a specific transcriptional response in $LXR^{-/-}$ mice that included altered cholesterol and bile acid homeostasis. ELISA showed that these effects were associated with an elevated FB1 concentration in the plasma of $LXR^{-/-}$ mice, suggesting that LXRs participate in intestinal absorption and/or clearance of the toxin. In summary, this study demonstrates an important role of LXRs in protecting the liver against FB1-induced toxicity, suggesting an alternative mechanism not related to the inhibition of sphingolipid synthesis for mycotoxin toxicity.

INTRODUCTION

Fumonisin B1 (FB1) is the most abundant and most documented mycotoxin of the fumonisin family, which contains more than 30 species (Wan Norhas et al. 2009). FB1 is produced mainly by *Fusarium verticillioides* and *Fusarium proliferatum* and mainly contaminates corn. As FB1 is nephrotoxic and hepatotoxic (Voss et al. 1995; Bondy et al. 1997; Humphreys et al. 2001) and exhibits deleterious effects on human and animal health, contamination levels are strictly regulated in food and feed ((Ec) No 1126/2007 Commission Regulation 2007; (Ec) No 576/2006 Commission Recommendation 2006). Other specific related clinical diseases include leukoencephalomalacia, pulmonary edema, cardiac dysfunction (Haschek et al. 2001), carcinogenesis (FAO/WHO 2001), neural tube defects (Marasas et al. 2004), and disruption of the intestines and immune system (Devriendt et al. 2009; Grenier et al. 2012).

Due to its structural similarity to sphingoid species, such as sphinganine (Sa) and sphingosine (So), FB1 represents an important competitive substrate for all ceramide synthases (Cers) involved in the formation of long-chain and very long-chain ceramides. Though FB1 decreases the quantity of ceramide and sphingomyelin species in tissues, it also increases the levels of Sa and sphingolipid terminal products, such as Sa 1-phosphate. Thus, the Sa/So ratio is used as a biomarker of exposure to FB1 in animals (Wang et al. 1991; Loiseau et al. 2007, 2015).

Several studies have reported a link between sphingolipids and the metabolism of other lipids, such as sterols and fatty acids. In the white adipose tissue of rats, *Cers4* has been identified as a potent target of modulators of endogenous lipid metabolism, such as leptin (Bonzón-Kulichenko et al. 2009), insulin, or changes in phospholipid transfer protein activity (PLTPα) (Rosenthal et al. 2011; Stratford et al. 2001). Moreover, fatty acid elongase 1 (ELOVL1) activity, which is particularly involved in saturated and monounsaturated C20- and C22-CoA synthesis, is regulated by CerS2, which is essential for the production of C24-sphingolipids (Ohno et al. 2010). Sphingomyelins have also been shown to be involved in the post-

translational regulation of master regulators of fatty acid and cholesterol metabolism, called sterol regulatory element-binding proteins (SREBPs), through inhibition of SREBP cleavage-activating protein (SCAP) (Scheek et al. 1997).

We recently reported that the kinome and transcriptome profiles of piglets exposed to toxic levels of FB1 revealed that most of the effects of the mycotoxin were mediated by the regulation of ceramide levels, which in turn influence protein phosphatase 2 (PP2A) and the phosphoinositide 3-kinase (PI3K)/AKT signaling pathways (Régnier et al. 2017). This disturbance induces inhibition of integrin-mediated cell-matrix adhesion, an inflammatory response, and alters the expression of genes involved in cholesterol and fatty acid homeostasis. We identified at least four modulated genes (*Abcg8*, *Scd1*, *Ldlr,* and *Fasn*) that are prototypical target genes regulated by the LXR nuclear receptors.

LXRs belong to the nuclear receptor superfamily, which comprises 48 members in humans and 49 in rodents (Gronemeyer et al. 2004). Two isoforms of LXR have been described: LXR_{α} (NR1H3) and LXR_{β} (NR1H2) (Teboul et al. 1995). These nuclear receptors are involved in cholesterol and fatty acid metabolism (Ducheix et al. 2013). $LXR_{\alpha}^{-/-}$, $LXR_{\beta}^{-/-}$, or $LXR_{\alpha/\beta}^{-/-}$ mice have shown an accumulation of cholesterol esters in the liver related to a defect in cholesterol excretion (Peet et al. 1998). In the intestine, LXRs limit cholesterol absorption by inducing the expression of ABC transporters G5 and G8 (Yu et al. 2005; Liqing Yu et al. 2003) and facilitates cholesterol excretion in high density lipoproteins (HDLs) by stimulating *Abca1*. In the liver, LXRs stimulate *Abcg5* and *Abcg8*, which is necessary for the excretion of cholesterol in the bile duct, and *Cyp7a1*, which is responsible for the degradation of cholesterol into biliary acids. These findings suggest that LXRs play an important role in the detoxification of FB1, but this has never been demonstrated. The aim of the present study was to compare the toxicity of FB1 in wild-type ($LXR^{+/+}$) and $LXR_{\alpha,\beta}$-deficient ($LXR^{-/-}$) mice. Our data indicate that LXRs control the plasmatic levels of plasmatic FB1 and, therefore, its toxicity in the liver.

MATERIALS AND METHODS

Animals

Female LXRα,β-/- double-deficient (LXR-/-) and LXRα,β+/+ mice (LXR+/+) with a mixed C57BL6J/129SVJ genetic background were bred at INRA's transgenic rodent facility at 22± 2°C. Animals were 8 weeks old at the beginning of the experiment and given free access to water and a basal diet (Harlan). Based on the literature, female mice were used in this study because of their higher sensitivity to FB1 compared to male mice (Bondy et al. 1997; Howard et al. 2001; Johnson and Sharma 2001). The experiments were carried out in accordance with the European Guidelines for the Care and Use of Animals for Research Purposes (accreditation number APAFIS#5917-2016070116429578).

Treatment with fumonisin B1

$LXR^{-/-}$ and $LXR^{+/+}$ mice were randomly divided into two groups of eight mice each. For the FB1 treated group, the drinking water was supplemented with fumonisin B1 (10 mg FB1/kg bw/day) for 4 weeks. Body weight and water intake were recorded weekly to adjust the quantity of FB1 in the water for changes in body weight and water consumption. At the end of the experiment, the mice were euthanized to collect blood and tissue samples. The liver was removed, dissected, snap-frozen in liquid nitrogen, and stored at -80°C until use.

Gene expression studies

Total RNA was extracted from the liver using Trizol® reagent (Amresco, USA). Gene expression profiles of six liver samples per group, randomly chosen, were obtained at the GeTTRiX facility (GénoToul, Génopole Toulouse Midi-Pyrénées) using Agilent Sureprint G3 Mouse GE v2 microarrays (8x60K, design 074809) following the manufacturer's instructions. For each sample, cyanine-3 (Cy3) labeled cRNA was prepared from 200 ng of total RNA using the One-Color Quick Amp Labeling kit (Agilent Technologies, California) according to the manufacturer's instructions, followed by Agencourt RNAClean XP (Agencourt Bioscience

Corporation, Massachusetts). Dye incorporation and cRNA yield were checked using a Dropsense™ 96 UV/VIS droplet reader (Trinean, Belgium). A total of 600 ng of Cy3-labeled cRNA were hybridized onto the microarray slides following the manufacturer's instructions. Immediately after washing, the slides were scanned on an Agilent G2505C Microarray Scanner using Agilent Scan Control A.8.5.1 software and the fluorescence signal extracted using Agilent Feature Extraction software v10.10.1.1 with default parameters. Microarray data and experimental details are available in NCBI's Gene Expression Omnibus (Edgar et al. 2002) and are accessible through GEO Series accession number GSE118072 (https://www.ncbi.nlm.nih.gov/geo/query/acc.cgi?acc=GSE118072).

For real-time quantitative polymerase chain reaction (qPCR), total RNA samples (2 µg) were reverse-transcribed using the High Capacity cDNA Reverse Transcription Kit (Applied Biosystems, California). Primers for Sybr Green assays are presented in Online Resource 1. Amplification reactions were performed on an ABI Prism 7300 Real Time PCR System (Applied Biosystem). The qPCR data were normalized to proteasome subunit beta type-6 (psmb6) mRNA levels and analyzed by LinRegPCR software.

Plasma analysis

Plasma levels of aspartate transaminase (AST), alanine transaminase (ALT), bilirubin, alkaline phosphatase, total cholesterol, LDL-cholesterol, and HDL-cholesterol were determined on a biochemical analyzer COBAS-MIRA+. Plasma FB1 concentrations were assayed using the Fumonisin ELISA Kit (Novakits, Nantes, France) following the manufacturer's instructions. The fumonisin ELISA (LOD = 2 µg/mL in plasma) uses antibodies raised in mouse against protein conjugated FB1. Plasmas were diluted by two in dilution buffer before ELISA assay. The optical density was measured at 450nm and 590nm using ELISA 96-well plate reader (TECAN). The concentration of FB1 in the plasma samples (pg/ml) corresponding to the maximal absorbance of each extract was read from the calibration curve ($R^2 = 0.9998$).

Biochemical assays

Total lipid extraction

Liver samples were homogenized in 1 ml of methanol/5 mM EGTA (2:1 v/v) with FastPrep-24™ (MP-Biomedicals, USA). Lipids corresponding to an equivalent of 2 mg of tissue were extracted according to Bligh and Dyer method (Bligh and Dyer 1959) in chloroform/methanol/water (2.5:2.5:2, v/v/v) in the presence of the internal standards. The solution was centrifuged at 1500 rpm for 3 min. The organic phase was collected and dried under nitrogen and then dissolved in an adequate eluent.

Neutral lipids

Neutral lipids were extracted as described above in the presence of including internal standards: 16 µg glyceryltrinonadecanoate, 6 µg stigmasterol, and 6 µg cholesteryl heptadecanoate (Sigma, Saint-Quentin-Fallavier, France). Total lipids were suspended in 160 µl of ethyl acetate and triglycerides, free cholesterol, and cholesterol esters analyzed by gas-liquid chromatography on a focus Thermo Electron system using a Zebron-1 Phenomenex fused-silica capillary column (5 m, 0.32 mm i.d., 0.50 mm film thickness). The oven temperature was programmed from 200 to 350°C at a rate of 5°C/min, and the carrier gas was hydrogen (0.5 bar), whereas the injector and detector temperatures were set at 315°C and 345°C, respectively. (Régnier et al. 2017b)

Ceramide, sphingomyelin, sphingosine, and sphinganine

Sphingolipids were extracted using the same protocol as neutral lipids using dichloromethane/water/methanol (2% acetic acid) (2.5:2:2.5, v/v/v) with the addition of internal standards: ceramide d18:1/15:0 (16 ng), sphingomyelin d18:1/12:0 (16 ng), sphingosine 17:0, and sphinganine 17:0. Sphingolipids and internal standards were analyzed by triple quadrupole mass spectrometry (QqQ MS) (Loiseau et al. 2015).

Histology

Hematoxylin/eosin staining was performed on tissue sections (5 µm) from paraformaldehyde-fixed, paraffin-embedded liver samples. Visualization was made possible using a Leica microscope DM4000 B equipped with a LEICA DFC450 C camera (Leica microsystems). Livers were examined by light microscopy. First, the 32 liver sections (one slide per animal, 8 slides per group, and four groups) were full-blinded screened by two persons to determine the effects present for each section. Inflammatory foci (corresponding to a minimum of 5 inflammatory cells), apoptotic bodies, cell injury, and mitosis were counted in 10 distinct areas on the 200x field for each liver slice (corresponding to an average number of 600 cells) and were approved by an histopathologist (T.A.S). Values were presented as the mean of 10 fields/slice. Next, Sirius red staining was performed on tissue sections (5 µm) from formalin-fixed, paraffin-embedded liver pieces and collagen fibers stained red.

Statistical analysis

For transcriptomic, histologic, and biochemical analyses, statistical analyses were performed using Graphpad Prism for Windows (version 7.00, Graphpad software). The data were expressed as mean ± SEM. Differential effects were analyzed by two-way analyse of variance (ANOVA) followed by appropriate posthoc tests (Sidak). A p-value < 0.05 was considered significant.

Microarray data were analyzed using R ("R: a language and environment for statistical computing" 2008) and Bioconductor packages (www.bioconductor.org, v 3.0) (Gentleman et al. 2004) as described in GEO accession GSE118072. Raw data (median signal intensity) were filtered, log2 transformed, corrected for batch effects (microarray washing bath and labeling serials), and normalized using the quantile method (Bolstad et al. 2003) A model was fitted using the limma lmFit function (Smyth 2004). Pair-wise comparisons between biological

conditions were applied using specific contrasts to extract simple genotype and treatment effects, but also interaction terms genotype:treatment. A correction for multiple testing was applied using the Benjamini-Hochberg procedure (Benjamini and Hochberg 1995) to control the false discovery rate (FDR). Hierarchical clustering was applied to the samples and differentially expressed probes using the 1-Pearson correlation coefficient as distance and Ward's criterion for agglomeration. The clustering results are illustrated as a heatmap of expression signals. Enrichment of Gene Ontology (GO) Biological Processes was performed using the GOC API included on the string-db.org website (Szklarczyk et al. 2015).

RESULTS

Physiological follow-up during FB1 exposure

Exposure to FB1 for 28 days had no effect on the body weight of the mice regardless of the genotype ($LXR^{+/+}$ or $LXR^{-/-}$), whereas significant effects of genotype on body weight were observed (Fig. 1A). Similarly, no change in food and water intake was observed during the experiment. However, an increase in body weight and water intake was observed in $LXR^{-/-}$ mice compared to $LXR^{+/+}$ mice (Fig. 1B). Though body weight remained unchanged, FB1 exposure led to decreased liver weight and increased spleen weight (Fig. 1C).

FB1 alters sphingolipid homeostasis in $LXR^{+/+}$ and $LXR^{-/-}$ mice

FB1 is a known pharmacological inhibitor of ceramide synthesis. The role of LXRs in the FB1-induced alteration of sphingolipid metabolism was investigated and several liver sphingolipids, such as ceramides, sphingomyelins, sphinganine, and sphingosine, measured in mice.

In both mouse strains, the sphingoid bases Sa and So were increased during FB1 exposure. Nevertheless, the increase in the Sa/So ratio was slightly greater in the $LXR^{-/-}$ mice than the $LXR^{+/+}$ mice (Fig. 2A).

Upon FB1 exposure, ceramide levels were decreased by 59% and 71% in the livers of $LXR^{+/+}$ and $LXR^{-/-}$ mice, respectively (Fig. 2B). Levels were significantly lower in $LXR^{-/-}$ mice than in $LXR^{+/+}$ mice, but FB1 exposure had the same effect in both $LXR^{+/+}$ and $LXR^{-/-}$ mice (no significant genotype/treatment interaction). When each ceramide species was measured, a decrease was observed in FB1-exposed mice regardless of genotype ($LXR^{-/-}$ or $LXR^{+/+}$) (Fig. 2D).

Similarly, FB1 exposure led to a decreased level of sphingomyelin in the liver in both $LXR^{+/+}$ and $LXR^{-/-}$ mice (Fig. 2B). Analyzing the effect of both genotype and the treatment on each

sphingomyelin species, a significant decrease in SM(d18:1/16:0), SM(d18:1/16:1), and SM(d18:1/22:1) and an increase in SM(d18:1/24:0) and SM(d18:1/24:1) were observed among FB1-treated mice. Moreover, a significant genotype effect was observed with a decrease in SM(d18:1/22:0) and an increase in SM(d18:1/24:1) (Fig. 2E). These results clearly show that FB1-associated inhibition of ceramide synthesis is not dependent on the LXR.

LXRs control the plasma FB1 concentration

LXRs regulate cholesterol efflux from enterocytes and their absence alter the efficiency of the tight junctions, resulting in an increase in plasma levels of cholesterol. We previously showed that LXR pathway is activated by FB1 (Régnier et al. 2017). In order to test if LXRs also participate to the modulation of plasma levels of FB1, plasma FB1 concentrations were measured in treated and untreated LXR +/+ and LXR -/- mice. We observed that $LXR^{-/-}$ mice treated with FB1 contained significantly higher concentrations of toxin compared to $LXR^{+/+}$ (Fig. 3). Even though we previously showed that sphingolipid inhibition by FB1 occurs independently of LXR, this result shows that LXR-dependent activity controls the bioavailability of FB1.

Effect of FB1 exposure on the hepatic gene expression profile

In order to investigate the changes in gene expression associated with the increase in plasma levels of FB1 combined with the absence of the LXR nuclear receptor, a microarray analysis was performed on the livers of $LXR^{+/+}$ and $LXR^{-/-}$ mice in the presence and absence of FB1 exposure. The statistical analysis identified thousands of genes regulated in response to FB1 in each mouse strain or differentially regulated between strains. The heatmap illustrated in Fig. 4A is generated by the selection of the top 2000 most significantly differentially expressed

probes for each contrast (based on adjusted p-value; FDR≤5%) corresponding to 4825 probes overall.

Four main clusters showing specific gene expression profiles according to experimental conditions have been identified from the hierarchical clustering of probes. Two of them (clusters 2 and 4) illustrate a genotype effect and the last two (clusters 1 and 3) reflect an effect of FB1 exposure.

Clusters 2 and 4 represent genes induced and repressed, respectively, in the absence of LXR, but not dependent on FB1 exposure (Fig. 4A). The biological function analysis of cluster 2 revealed that LXR deficiency induces cytokine receptor interaction and catalytic activities, such as the characteristic gene *Cyp2b10*. In line with the role of LXR in lipid metabolism, biological function analyses of cluster 4 revealed that LXR deficiency influences the PPAR signaling pathway, pyruvate, and fatty acid metabolism. A representative LXR target gene is sterol regulatory element-binding transcription factor 1-c (*Srebp1-c*). Its expression is significantly decreased in the absence of LXR, regardless of treatment (Fig. 4B).

Clusters 1 and 3 represent a panel of genes whose expression is sensitive to FB1 (Fig. 4A). Biological function analysis of cluster 1 revealed that the main FB1-activated pathways are focal adhesion, PI3K-AKT signaling pathways, proteoglycans in cancers, ECM-receptor interaction, and chronic myeloid leukemia (Fig. 4B and Online Resource 2). Using qPCR, we measured the expression of a fibrosis reference gene, collagen, type I, alpha 1 (*Col1a1*), a representative gene of cluster 1. *Col1a1* was induced only in $LXR^{-/-}$ mice treated with FB1 (Fig. 4B). In contrast, FB1 reduced the expression of genes included in cluster 3 and involved in metabolic pathways, amino acid degradation, amino acid metabolism, drug metabolism, and bile secretion (Fig. 4B and Online Resource 3). For example, expression of UDP glucuronosyltransferase 2 family, polypeptide B1 (*Ugt2b1*), involved in drug metabolism and bile secretion is significantly decreased in $LXR^{-/-}$ mice treated with FB1.

LXR deficiency influences the hepatic gene expression profile in response to FB1

A Venn diagram was used to highlight LXR-dependent changes during FB1 treatment (Fig. 5A). Among the significant DEGs related to FB1, 40 were specific to $LXR^{+/+}$ mice (34 up-regulated genes and 6 down-regulated genes) and 6056 were specific to $LXR^{-/-}$ mice (3026 up-regulated and 3020 down-regulated). Thus, LXR deficiency reveals a broad range of FB1-sensitive genes (Fig. 5A). The 40 genes with the highest changes in hepatic gene expression in the livers of $LXR^{-/-}$ mice (blue bars Fig. 5B and 5C) differed from those observed $LXR^{+/+}$ mice (red bars Fig. 5B and 5C). Most of these genes are involved in inflammation, fibrogenesis, and carcinogenesis, including *Cd63* antigen, *Col1a1*, *Col3a1*, chemokine (C-X-C motif) ligand 14 (*Cxcl14*), and Ras-related protein RAB7 (*Rab7b*) (Fig. 5B). Conversely, the 40 genes reduced by FB1 in $LXR^{-/-}$ mice were largely involved in bile secretion and drug metabolism (Fig. 5C). Measuring the expression of some genes by qPCR revealed that *Col1a1*, *Elovl7* (involved in the elongation of very long-chain fatty acids protein 7), and *Smpd3* (neutral sphingomyelinase) are largely up-regulated in response to FB1 in the absence of LXR, whereas, steroid 7-alpha-hydroxylase (*Cyp7b1*), transmembrane 7 superfamily member 2 (*Tm7sf2*), and ATP binding cassette subfamily G member 8 (*Abcg8*), involved in lipid and bile acid metabolism were down-regulated by FB1 (Fig. 5D).

LXR deficiency alters liver biochemistry in response to FB1

As many genes are modulated by FB1 exposure in $LXR^{-/-}$ mice, plasma biochemistry analysis was performed to investigate the metabolic consequences of the toxin. As shown in Fig. 6A, exposure to FB1 was associated with a greater increase in plasma alanine amino transferase (ALT), aspartate amino transferase (AST), and alkaline phosphatase (ALP) in $LXR^{-/-}$ mice than $LXR^{+/+}$ mice (4-, 3-, and 2-fold, respectively). In addition, FB1 treatment increased plasma bilirubin levels 3- and 2-fold in $LXR^{+/+}$ and $LXR^{-/-}$ mice, respectively.

FB1 exposure also induced a significant increase in plasma levels of HDL, LDL, and total cholesterol in $LXR^{-/-}$ mice, but did not modulate the plasma level of these lipoproteins in $LXR^{+/+}$ mice (Fig. 6B). Because the accumulation of cholesterol can be hepatotoxic, we investigated the effect of FB1 on liver cholesterol. As expected, an accumulation of hepatic cholesterol and cholesterol esters was observed in LXR-deficient mice compared to wild-type mice (Fig. 6C); however, exposure to FB1 did not have significant effects on the levels of these metabolites. Interestingly, hepatic triglyceride levels were reduced in $LXR^{-/-}$ mice and further decreased by FB1 (Fig. 6C).

LXR deficiency enhances liver injury in response to FB1

The severity of liver lesions associated with altered plasma biochemistry were assessed on hematoxylin and eosin and Sirius red stained tissues. Livers from $LXR^{+/+}$ mice exposed to FB1 exhibited a small increase in histological lesions, particularly those associated with apoptosis, inflammatory foci, and mitosis. Nevertheless, differences from the unexposed $LXR^{+/+}$ mice were not significant. In comparison, livers from unexposed $LXR^{-/-}$ mice exhibited macrophage infiltration and tissue fibrosis (Fig. 7A). The histopathological changes in the liver of $LXR^{-/-}$ treated mice with FB1, in comparison with control group, are characterized by obvious increase in degenerative changes and apoptotic cells in comparison with control group.

DISCUSSION

The aim of this study was to question the role of the nuclear LXRs in the toxicity of mycotoxin FB1. Modulation of the LXR pathway by FB1 in the liver of piglets was described in a previous study using untargeted (transcriptomic and phospho-proteomic) approaches (Régnier et al. 2017). In the current study, the role of LXRs in FB1 toxicity was assessed using $LXR^{+/+}$ and $LXR^{-/-}$ mice. Though we observed no effect of LXRs on the inhibition of ceramide synthesis, we demonstrated that LXRs protect against FB1-induced liver damage.

First, we demonstrated that exposure to the toxin does not affect body weight or food and water consumption by the mice (Fig. 1), unlike what has been observed in other animal species, such as pigs (Marin et al. 2006; Régnier et al. 2017). Interestingly, though the body weights of mice remained unchanged, FB1 exposure decreased liver weight while increasing the spleen weight. These physiological changes are in accordance with previous results from our lab and other, revealing that FB1 alters hepatic lipogenesis and immune responses (Devriendt et al. 2009; Régnier et al. 2017).

In $LXR^{+/+}$ and $LXR^{-/-}$ mice, FB1 exposure significantly decreased total ceramide content, including 10 different ceramide species. These results are consistent with the transcriptomic analyses of the expression of ceramide synthase 2 (*Cers2*) and sphingomyelin phosphodiesterase 1 *(Smpd1*), two enzymes involved in sphingolipid metabolism that are significantly inhibited by FB1 exposure, regardless of the presence of LXRs; the ceramide-inhibition rate was the same regardless of genotype. The decrease in ceramide due to the inhibition of ceramide synthase resulted in an increase in sphinganine and sphingosine levels as described in several other studies (Loiseau et al. 2015; Masching et al. 2016; Riedel et al. 2016; Régnier et al. 2017a). Notably, exposure to FB1 induced a rapid elevation in sphinganine, leading to a higher Sa/So ratio (Burel et al. 2013; Loiseau et al. 2007), whereas the increase in sphingosine levels only occurred at a later stage concomitantly with the alterations in the liver tissue (Wang et al. 1991). In the present study, we observed that a similar degree of ceramide reduction was achieved in both genotypes even though different FB1 plasma levels were observed. These results implied that FB1 inhibits ceramide synthesis more potently in $LXR^{+/+}$ mice, unless if the effect of FB1 on ceramide metabolism is already maximal in $LXR^{+/+}$ mice at the dose used in the present study. Although FB1 is poorly absorbed in the intestine and the majority of FB1 is excreted into the bile, the present study shows higher levels of FB1 in the

plasma of $LXR^{-/-}$ mice. We postulate that LXRs contribute directly to the bioavailability of FB1 by inhibiting its absorption in the intestine and/or increasing bile degradation in the liver.

The $LXR^{-/-}$ mouse model associated with the development of liver diseases provided an opportunity to investigate the effects of FB1 exposure. Beaven et al. demonstrated that $LXR^{-/-}$ mice are susceptible to liver fibrosis in different experimental models, whereas FB1 is also associated with the induction of liver fibrosis and injury (Voss et al. 1995; Howard et al. 2002). In order to investigate the specific liver damage induced by FB1 in $LXR^{-/-}$ mice, microarray analysis of the hepatic transcriptome was performed. Until now, only a few transcriptional pathways modulated by FB1 exposure have been characterized. Recently, we observed that exposure of pigs to FB1 for 1 month activates the AKT/PTEN pathway and decreases lipid metabolism. In the present study, both of these pathways were modulated by FB1, but these changes occurred specifically in the $LXR^{-/-}$ mice, suggesting that pigs are more sensitive to FB1 than mice and that LXR is critical in protecting mice against FB1-associated damages.

The modulation of the transcriptome by FB1 was more pronounced in $LXR^{-/-}$ mice than in $LXR^{+/+}$ mice, and the induction of characteristic genes of fibrosis, such as *Col1a1*, *Col3a1,* or *Anxa2,* became evident (Asselah et al. 2005; Yang et al. 2017). Overall, the main regulatory pathways increased by FB1 in $LXR^{-/-}$ mice involved carcinogenesis, actin regulation, and inflammation, confirming the critical role of LXRs in avoiding FB1 hepatotoxicity. Conversely, bile acid degradation appears as one of the most significative pathway down-regulated by FB1 in $LXR^{-/-}$ mice, suggesting that excretion of FB1 from the liver is impaired in absence of LXR.

To investigate hepatotoxicity in $LXR^{-/-}$ mice exposed to FB1, biochemical parameters were measured. An increase in plasma levels of AST, ALT, and alkaline phosphatase was observed in response to FB1 only in $LXR^{-/-}$ mice. These enzymes are predominantly expressed in hepatocytes, and the large increase in their plasma levels is associated with hepatocyte injury and necrosis (Scheig 1996; Schmidt and Schmidt 1993). These results underlined the

hepatotoxic effects of FB1 in absence of LXRs in mice. These findings have also been observed in high-dose FB1 exposure studies (National Toxicology Program 2001). Consistent with this point, histological analysis showed a specific increased in inflammation foci, necrosis, mitosis and fibrosis in $LXR^{-/-}$ mice exposed to FB1.Alongside, we showed that the absence of LXRs increased plasma levels of FB1, suggesting that exacerbated toxicity in LXR knockout mice is most likely attributed to the higher toxin levels in these animals..

In addition, FB1-treated $LXR^{-/-}$ mice exhibited elevated levels of plasma HDL-cholesterol, LDL-cholesterol, and total cholesterol characteristic of FB1-induced hepatotoxicity (Howard et al. 2002; Voss et al. 1995). Thus, we postulate that the absence of LXRs disrupts cholesterol metabolism and increases the bioavailability of FB1 *via* the intestine. A possible mechanism that can explain the role of LXRs in modulating the effects of FB1-toxicity may involve LPCAT3. LPCAT3 is a phospholipid remodeling enzyme under LXR control that modulates intestinal fatty acid and cholesterol absorption (Rong et al. 2013; Wang et al. 2016).

Overall, this study suggests that, in the absence of LXRs, FB1 accumulates in plasma and organs potentially through a defect in intestinal absorption and/or bile acid degradation. Therefore, LXRs act, at least in part, as regulators of the bioavailability of FB1. Thus, in the absence of LXRs, FB1 accumulates in the plasma and liver and induces deleterious effects, such as fibrosis and liver injury.

CONCLUSION

Our results show that LXRs are critical to preventing toxic effects associated with FB1 exposure. Previous studies suggested that sphingolipids act as mediators of FB1 toxicity (Benlasher et al. 2012; Merrill et al. 1996; Riley et al. 2001) because these metabolites are involved in inflammatory processes and liver pathologies (Holland et al. 2011; Raichur et al. 2014; Turpin et al. 2014). Here, we highlight the key role of LXR in regulating FB1

bioavailability regardless of ceramide metabolism. LXR deficiency does not further enhance the inhibition of sphingolipid synthesis (ceramide, sphinganine, sphingosine, and sphingomyelin) by FB1, but has severe consequences on FB1-induced toxicity in the liver. This demonstrates that FB1 hepatotoxicity is not related solely to the inhibition of sphingolipid synthesis.

ACKNOWLEDGMENTS

MR was supported by a Fellowship from the Ministère de l'Education Nationale, de la Recherche et de la Technologie. This study was supported by the ANR Fumolip (ANR-16-CE21-0003) and ANR LipoReg (ANR-15-Carn0016), France. We thank Dr. David J. Mangelsdorf (Howard Hughes Medical Institute, Dallas, TX) for providing us with the LXR-deficient mice and for constructive discussions. We thank all members of the EZOP staff. We thank Aurore Laurent Monbrun for his excellent work on plasma biochemistry. We also thank the staff from the Genotoul: Anexplo, GeT-TriX, and Metatoul-Lipidomic facilities.

CONFLICT OF INTEREST

The authors declare that they have no conflict of interest.

REFERENCES :

(Ec) No 1126/2007 Commission Regulation (2007) COMMISSION REGULATION (EC) No 1126/2007

(Ec) No 576/2006 Commission Recommendation (2006) COMMISSION RECOMMENDATION (EC) No 576/2006

Asselah T, Bièche I, Laurendeau I, et al (2005) Liver gene expression signature of mild fibrosis

in patients with chronic hepatitis C. Gastroenterology 129:2064–75. doi: 10.1053/j.gastro.2005.09.010

Benjamini Y, Hochberg Y (1995) Controlling the False Discovery Rate: A Practical and Powerful Approach to Multiple Testing. J. R. Stat. Soc. Ser. B 57:289–300

Benlasher E, Geng X, Xuan Nguyen NT, et al (2012) Comparative Effects of Fumonisins on Sphingolipid Metabolism and Toxicity in Ducks and Turkeys. Avian Dis 56:120–127. doi: 10.1637/9853-071911-Reg.1

Bligh EG, Dyer WJ (1959) A RAPID METHOD OF TOTAL LIPID EXTRACTION AND PURIFICATION. Can J Biochem Physiol 37:911–917. doi: 10.1139/o59-099

Bolstad BM, Irizarry RA, Astrand M, Speed TP (2003) A comparison of normalization methods for high density oligonucleotide array data based on variance and bias. Bioinformatics 19:185–93

Bondy GS, Suzuki CAM, Fernie SM, et al (1997) Toxicity of fumonisin B1to B6C3F1mice: A 14-day gavage study. Food Chem Toxicol 35:981–989. doi: 10.1016/S0278-6915(97)87267-5

Bonzón-Kulichenko E, Schwudke D, Gallardo N, et al (2009) Central leptin regulates total ceramide content and sterol regulatory element binding protein-1C proteolytic maturation in rat white adipose tissue. Endocrinology 150:169–78. doi: 10.1210/en.2008-0505

Burel C, Tanguy M, Guerre P, et al (2013) Effect of low dose of fumonisins on pig health: immune status, intestinal microbiota and sensitivity to Salmonella. Toxins (Basel) 5:841–64. doi: 10.3390/toxins5040841

Devriendt B, Gallois M, Verdonck F, et al (2009) The food contaminant fumonisin B(1) reduces the maturation of porcine CD11R1(+) intestinal antigen presenting cells and antigen-specific immune responses, leading to a prolonged intestinal ETEC infection. Vet Res

40:40. doi: 10.1051/vetres/2009023

Ducheix S, Montagner A, Theodorou V, et al (2013) The liver X receptor: A master regulator of the gut–liver axis and a target for non alcoholic fatty liver disease. Biochem Pharmacol 86:96–105. doi: 10.1016/j.bcp.2013.03.016

Edgar R, Domrachev M, Lash AE (2002) Gene Expression Omnibus: NCBI gene expression and hybridization array data repository. Nucleic Acids Res 30:207–10

FAO/WHO (2001) Safety evaluation of certain mycotoxins in food

Gentleman RC, Carey VJ, Bates DM, et al (2004) Bioconductor: open software development for computational biology and bioinformatics. Genome Biol 5:R80. doi: 10.1186/gb-2004-5-10-r80

Grenier B, Bracarense A-PFL, Schwartz HE, et al (2012) The low intestinal and hepatic toxicity of hydrolyzed fumonisin B_1 correlates with its inability to alter the metabolism of sphingolipids. Biochem Pharmacol 83:1465–73. doi: 10.1016/j.bcp.2012.02.007

Gronemeyer H, Gustafsson J-Å, Laudet V (2004) Principles for modulation of the nuclear receptor superfamily. Nat Rev Drug Discov 3:950–964. doi: 10.1038/nrd1551

Haschek WM, Gumprecht LA, Smith G, et al (2001) Fumonisin toxicosis in swine: an overview of porcine pulmonary edema and current perspectives. Environ Health Perspect 109 Suppl:251–7

Holland WL, Bikman BT, Wang L-P, et al (2011) Lipid-induced insulin resistance mediated by the proinflammatory receptor TLR4 requires saturated fatty acid–induced ceramide biosynthesis in mice. J Clin Invest 121:1858–1870. doi: 10.1172/JCI43378

Howard PC, Couch LH, Patton RE, et al (2002) Comparison of the toxicity of several fumonisin derivatives in a 28-day feeding study with female B6C3F(1) mice. Toxicol Appl

Pharmacol 185:153–65

Howard PC, Eppley RM, Stack ME, et al (2001) Fumonisin b1 carcinogenicity in a two-year feeding study using F344 rats and B6C3F1 mice. Environ Health Perspect 109:277–282. doi: 10.1289/ehp.01109s2277

Humphreys SH, Carrington C, Bolger M (2001) A quantitative risk assessment for fumonisins B1 and B2 in US corn. Food Addit Contam 18:211–20. doi: 10.1080/02652030010021486

Johnson V., Sharma R. (2001) Gender-dependent immunosuppression following subacute exposure to fumonisin B1. Int Immunopharmacol 1:2023–2034. doi: 10.1016/S1567-5769(01)00131-X

Loiseau N, Debrauwer L, Sambou T, et al (2007) Fumonisin B1 exposure and its selective effect on porcine jejunal segment: Sphingolipids, glycolipids and trans-epithelial passage disturbance. Biochem Pharmacol 74:. doi: 10.1016/j.bcp.2007.03.031

Loiseau N, Polizzi A, Dupuy A, et al (2015) New insights into the organ-specific adverse effects of fumonisin B1: comparison between lung and liver. Arch Toxicol 89:1619–1629. doi: 10.1007/s00204-014-1323-6

Marasas WFO, Riley RT, Hendricks KA, et al (2004) Fumonisins Disrupt Sphingolipid Metabolism, Folate Transport, and Neural Tube Development in Embryo Culture and In Vivo: A Potential Risk Factor for Human Neural Tube Defects among Populations Consuming Fumonisin-Contaminated Maize. J Nutr 134:711–716. doi: 10.1093/jn/134.4.711

Marin DE, Taranu I, Pascale F, et al (2006) Sex-related differences in the immune response of weanling piglets exposed to low doses of fumonisin extract. Br J Nutr 95:1185–92

Masching S, Naehrer K, Schwartz-Zimmermann H-E, et al (2016) Gastrointestinal Degradation of Fumonisin B1 by Carboxylesterase FumD Prevents Fumonisin Induced Alteration of

Sphingolipid Metabolism in Turkey and Swine. Toxins (Basel) 8:84. doi: 10.3390/toxins8030084

Merrill AH, Wang E, Vales TR, et al (1996) Fumonisin toxicity and sphingolipid biosynthesis. Adv Exp Med Biol 392:297–306

National Toxicology Program (2001) IN F344/N RATS AND B6C3F 1 MICE

Ohno Y, Suto S, Yamanaka M, et al (2010) ELOVL1 production of C24 acyl-CoAs is linked to C24 sphingolipid synthesis. Proc Natl Acad Sci U S A 107:18439–44. doi: 10.1073/pnas.1005572107

Peet DJ, Turley SD, Ma W, et al (1998) Cholesterol and bile acid metabolism are impaired in mice lacking the nuclear oxysterol receptor LXR alpha. Cell 93:693–704

Raichur S, Wang ST, Chan PW, et al (2014) CerS2 Haploinsufficiency Inhibits β-Oxidation and Confers Susceptibility to Diet-Induced Steatohepatitis and Insulin Resistance. Cell Metab 20:687–695. doi: 10.1016/j.cmet.2014.09.015

Régnier M, Gourbeyre P, Pinton P, et al (2017a) Identification of Signaling Pathways Targeted by the Food Contaminant FB1: Transcriptome and Kinome Analysis of Samples from Pig Liver and Intestine. Mol Nutr Food Res 61:1700433. doi: 10.1002/mnfr.201700433

Régnier M, Polizzi A, Lippi Y, et al (2017b) Insights into the role of hepatocyte PPARα activity in response to fasting. Mol Cell Endocrinol. doi: 10.1016/j.mce.2017.07.035

Riedel S, Abel S, Burger H-M, et al (2016) Differential modulation of the lipid metabolism as a model for cellular resistance to fumonisin B1–induced cytotoxic effects in vitro. Prostaglandins, Leukot Essent Fat Acids 109:39–51. doi: 10.1016/j.plefa.2016.04.006

Riley RT, Enongene E, Voss KA, et al (2001) Sphingolipid perturbations as mechanisms for fumonisin carcinogenesis. Environ Health Perspect 109 Suppl 2:301–8

Rong X, Albert CJ, Hong C, et al (2013) LXRs Regulate ER Stress and Inflammation through Dynamic Modulation of Membrane Phospholipid Composition. Cell Metab 18:685–697. doi: 10.1016/j.cmet.2013.10.002

Rosenthal EA, Ronald J, Rothstein J, et al (2011) Linkage and association of phospholipid transfer protein activity to *LASS4*. J Lipid Res 52:1837–1846. doi: 10.1194/jlr.P016576

Scheek S, Brown MS, Goldstein JL (1997) Sphingomyelin depletion in cultured cells blocks proteolysis of sterol regulatory element binding proteins at site 1. Proc Natl Acad Sci U S A 94:11179–83

Scheig R (1996) Evaluation of tests used to screen patients with liver disorders. Prim Care 23:551–60

Schmidt E, Schmidt FW (1993) Enzyme diagnosis of liver diseases. Clin Biochem 26:241–51

Stratford S, DeWald DB, Summers SA (2001) Ceramide dissociates 3'-phosphoinositide production from pleckstrin homology domain translocation. Biochem J 354:359–68

Szklarczyk D, Franceschini A, Wyder S, et al (2015) STRING v10: protein–protein interaction networks, integrated over the tree of life. Nucleic Acids Res 43:D447–D452. doi: 10.1093/nar/gku1003

Teboul M, Enmark E, Li Q, et al (1995) OR-1, a member of the nuclear receptor superfamily that interacts with the 9-cis-retinoic acid receptor. Proc Natl Acad Sci U S A 92:2096–100

Turpin SM, Nicholls HT, Willmes DM, et al (2014) Obesity-Induced CerS6-Dependent C16:0 Ceramide Production Promotes Weight Gain and Glucose Intolerance. Cell Metab 20:678–686. doi: 10.1016/j.cmet.2014.08.002

Voss KA, Chamberlain WJ, Bacon CW, et al (1995) Subchronic Feeding Study of the Mycotoxin Fumonisin B1 in B6C3F1 Mice and Fischer 344 Rats. Fundam Appl Toxicol

24:102–110. doi: 10.1006/FAAT.1995.1012

Wan Norhas WM, Abdulamir AS, Abu Bakar F, et al (2009) The Health and Toxic Adverse Effects of Fusarium Fungal Mycotoxin, Fumonisins, on Human Population. Am J Infect Dis 5:273–281. doi: 10.3844/ajidsp.2009.273.281

Wang B, Rong X, Duerr MA, et al (2016) Intestinal Phospholipid Remodeling Is Required for Dietary-Lipid Uptake and Survival on a High-Fat Diet. Cell Metab 23:492–504. doi: 10.1016/j.cmet.2016.01.001

Wang E, Norred WP, Bacon CW, et al (1991) Inhibition of sphingolipid biosynthesis by fumonisins. Implications for diseases associated with Fusarium moniliforme. J Biol Chem 266:14486–90

Yang M, Wang C, Li S, et al (2017) Annexin A2 promotes liver fibrosis by mediating von Willebrand factor secretion. Dig Liver Dis 49:780–788. doi: 10.1016/j.dld.2017.02.013

Yu L, Gupta S, Xu F, et al (2005) Expression of ABCG5 and ABCG8 Is Required for Regulation of Biliary Cholesterol Secretion. J Biol Chem 280:8742–8747. doi: 10.1074/jbc.M411080200

Yu L, York J, von Bergmann K, et al (2003) Stimulation of Cholesterol Excretion by the Liver X Receptor Agonist Requires ATP-binding Cassette Transporters G5 and G8. J Biol Chem 278:15565–15570. doi: 10.1074/jbc.M301311200

(2008) R: a language and environment for statistical computing

Figure legends

Fig. 1 Physiological follow-up during FB1 exposure. $LXR^{+/+}$ or $LXR^{-/-}$ mice were exposed to FB1 at 10 mg/kg bw/day for 28 days. (a) Body weight was followed every week over the 28 days. (b) Daily food and water intake. (c) Liver and spleen weight relative to body weight after 28 days of exposure. Data are presented as mean ± SEM (n=8/group). T, significant treatment effect; G, significant genotype effect; TxG, significant interaction with $p \leq 0.05$

Fig. 2 FB1 alters sphingolipid homeostasis in $LXR^{+/+}$ and $LXR^{-/-}$ mice. $LXR^{+/+}$ or $LXR^{-/-}$ mice were exposed to FB1 at 10 mg/kg bw/day for 28 days. (a) Sphinganine and sphingosine levels in liver samples and the sphinganine (Sa)/sphingosine (So) ratio. (b) Ceramide and sphingomyelin levels in liver samples. (c) Relative mRNA expression of *CerS2* and *Smpd1* in liver samples quantified by qPCR. (d) Hepatic quantity of d18:1 ceramide species. (e) Hepatic quantity of d18:1 sphingomyelin species. Data are presented as mean ± SEM (n=8/group). T, significant treatment effect; G, significant genotype effect; TxG, significant interaction with $p \leq 0.05$

Fig. 3 LXR controls the plasma FB1 concentration. Plasma levels of fumonisin B1 in $LXR^{+/+}$ and $LXR^{-/-}$ mice. Data are presented as mean ± SEM (n=8/group). T, significant treatment effect; G, significant genotype effect; TxG, significant interaction with $p \leq 0.05$

Fig. 4 FB1 exposure leads to specific changes in the hepatic gene expression profile. $LXR^{+/+}$ or $LXR^{-/-}$ mice were exposed to FB1 at 10 mg/kg bw/day for 28 days. Gene expression profiles were analyzed in liver samples from $LXR^{+/+}$ or $LXR^{-/-}$ mice exposed to CTRL or FB1 (n=6/group) using Agilent microarrays. The top 2000 most significantly regulated probes (FDR≤5%), based on adjusted p–value, were selected for each contrast (5 contrasts and 4825

probes overall). (a) The gene expression profiles of 4825 probes are illustrated as a heatmap. Red and green indicate values above and below the mean averaged centered and scaled expression values (Z-score), respectively. Black indicates values close to the mean. According to the probe clustering (left panel), four gene clusters exhibited specific gene expression profiles, which are described on the right of the Heatmap. (b) Enriched Gene Ontology (GO) functions ($p \leq 0.01$) in each cluster and relative mRNA expression by qPCR of a gene that is characteristic of each cluster. qPCR data are presented as mean ± SEM (n=8/group). T, significant treatment effect; G, significant genotype effect; TxG, significant interaction with $p \leq 0.05$

Fig. 5 LXR deficiency influences the hepatic gene expression profile in response to FB1. (a) Veen diagram comparing differentially expressed genes (FDR≤1%) in response to FB1 exposure in $LXR^{+/+}$ and $LXR^{-/-}$ mice. Up-regulated genes and down-regulating genes are represented in bold and regular font, respectively. (b) and (c) panels are Bar plots representation of the Fold Change (in Log2) of the relative gene expression in response to FB1 exposure, for the top 40 most significant (FDR≤1%) up-regulated (b) or down-regulated (c) gene expression in LXR-/- mice (Blue bars) and in LXR+/+ mice (Red bars). (d) Relative gene expression of *Col1a1*, *Smpd3*, *Elovl7, Cyp7b1*, *Tm7sf2,* and *Abcg8* in liver samples quantified by qPCR. Data are presented as mean ± SEM (n=8/group). T, significant treatment effect; G, significant genotype effect; TxG, significant interaction with a $p \leq 0.05$

Fig. 6 LXR deficiency alters liver biochemistry in response to FB1. $LXR^{+/+}$ or $LXR^{-/-}$ mice were exposed to FB1 at 10 mg/kg bw/day for 28 days. (a) Plasma ALT, AST, ALP, and bilirubin levels. (b) Plasma cholesterol (HDL, LDL, and total). (c) Hepatic cholesterol, esterified cholesterol (EC), and triglyceride (TG) levels. Data are presented as mean ± SEM (n=8/group).

T, significant treatment effect; G, significant genotype effect; TxG, significant interaction with $p \leq 0.05$

Fig. 7 LXR deficiency enhances liver injury in response to FB1. $LXR^{+/+}$ or $LXR^{-/-}$ mice were exposed to FB1 at 10 mg/kg bw/day for 28 days. (a) Representative hematoxylin and eosin or Sirius red staining of liver sections. Scale bars, 100 μm. (b) Histological scoring of apoptosis, inflammatory foci, mitosis, and necrosis in 10 distinct areas from $LXR^{+/+}$ and $LXR^{-/-}$ mice exposed or not exposed to FB1. Field 200X. Data are presented as mean ± SEM (n=8/group). T, significant treatment effect; G, significant genotype effect; TxG, significant interaction with $p \leq 0.05$

Online Resource 1: Oligonucleotide sequences for real-time PCR

Online Resource 2: Pathways significantly up-regulated specifically in $LXR^{-/-}$ mice treated with FB1

Online Resource 3: Pathways significantly down-regulated specifically in $LXR^{-/-}$ mice treated with FB1

Figure 1

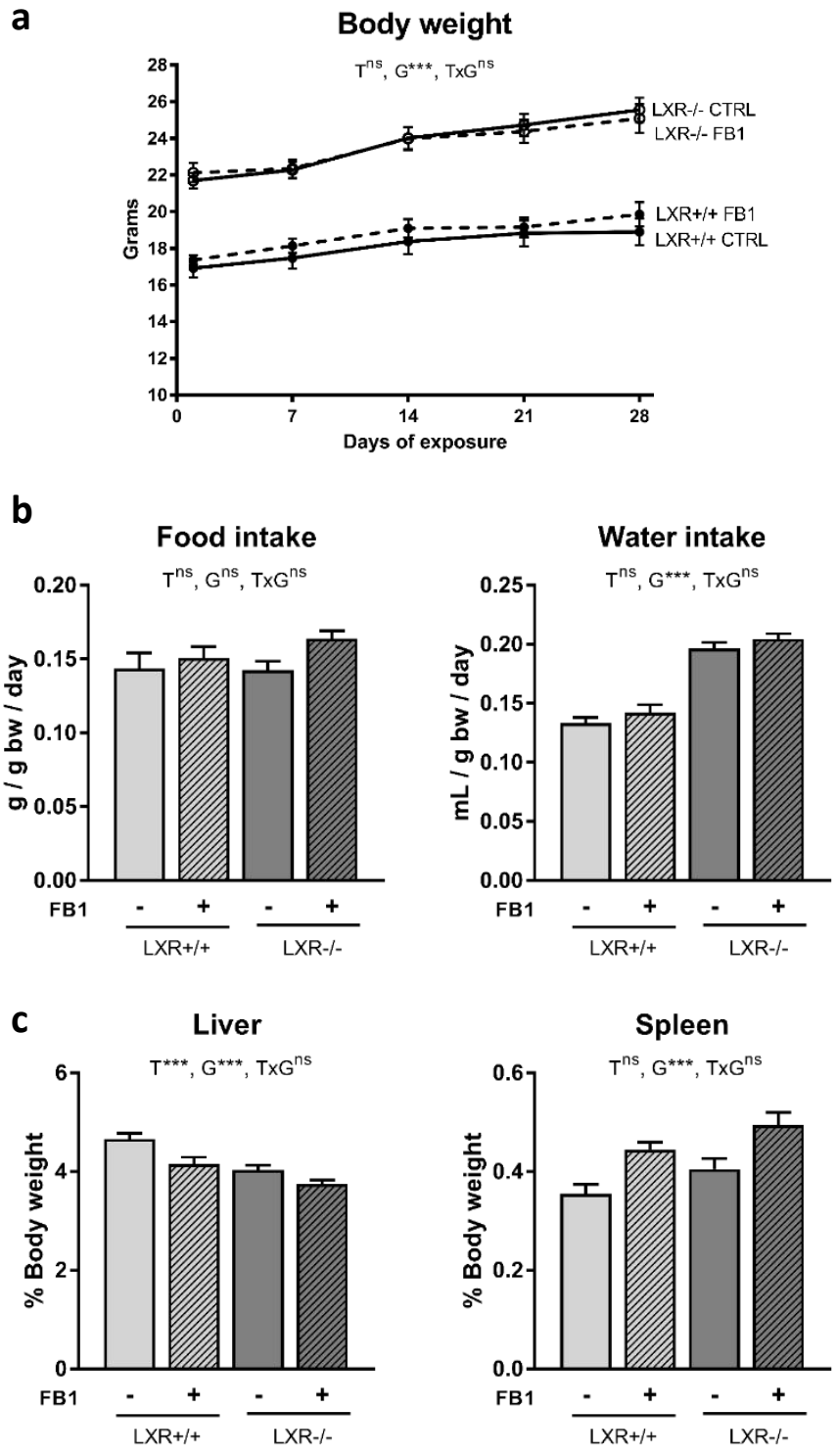
a
Body weight
T^ns, G***, TxG^ns
Grams
Days of exposure
LXR-/- CTRL
LXR-/- FB1
LXR+/+ FB1
LXR+/+ CTRL
b
Food intake
T^ns, G^ns, TxG^ns
g / g bw / day
Water intake
T^ns, G***, TxG^ns
mL / g bw / day
FB1
LXR+/+
LXR-/-
c
Liver
T***, G***, TxG^ns
% Body weight
Spleen
T^ns, G***, TxG^ns
% Body weight

Figure 2

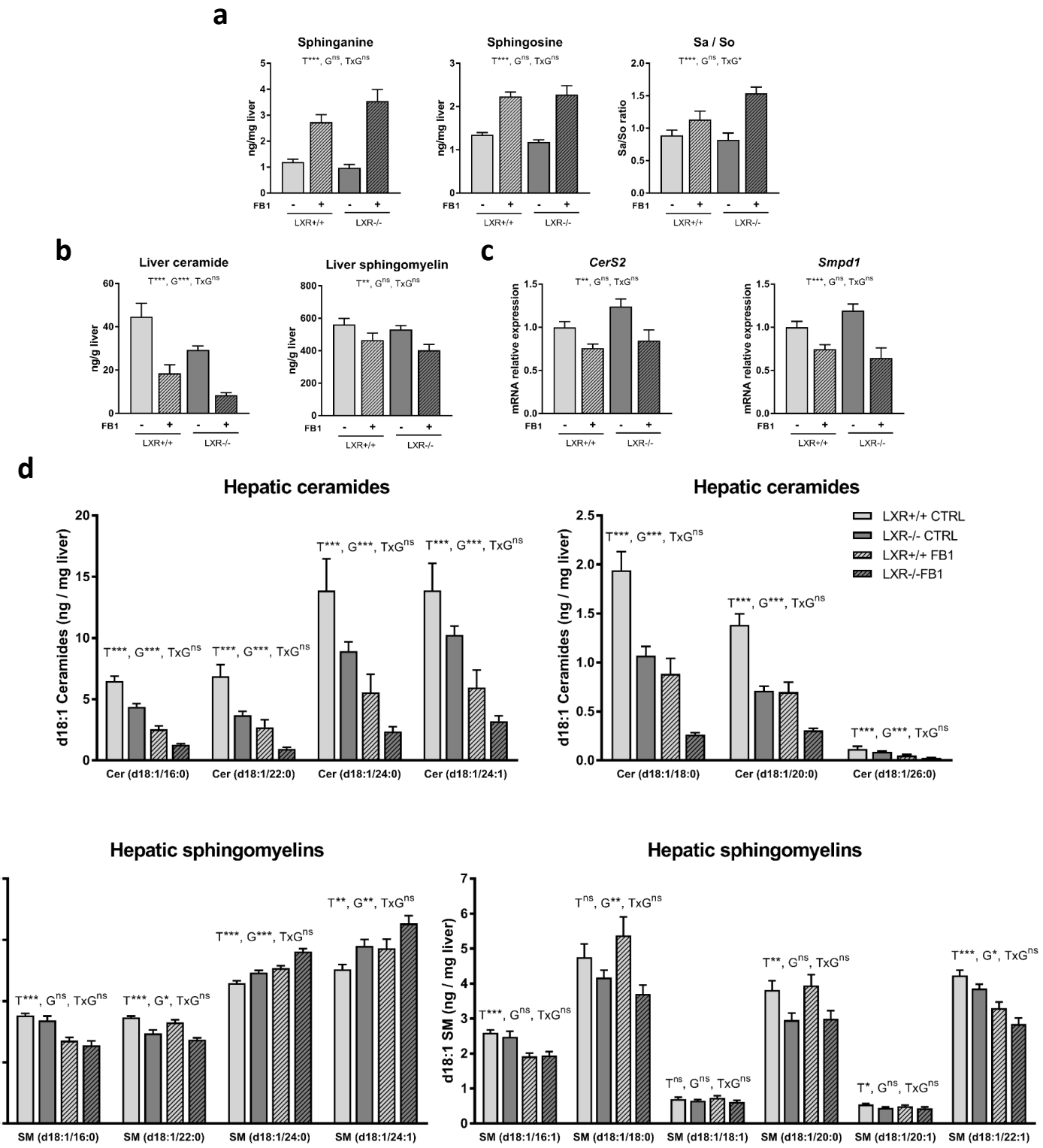
a
Sphinganine
T***, G^ns, TxG^ns
ng/mg liver
Sphingosine
T***, G^ns, TxG^ns
ng/mg liver
Sa / So
T***, G^ns, TxG*
Sa/So ratio
FB1
LXR+/+
LXR-/-
b
Liver ceramide
T***, G***, TxG^ns
ng/g liver
Liver sphingomyelin
T**, G^ns, TxG^ns
ng/g liver
c
CerS2
T**, G^ns, TxG^ns
mRNA relative expression
Smpd1
T***, G^ns, TxG^ns
mRNA relative expression
d
Hepatic ceramides
d18:1 Ceramides (ng / mg liver)
T***, G***, TxG^ns
Cer (d18:1/16:0)
Cer (d18:1/22:0)
Cer (d18:1/24:0)
Cer (d18:1/24:1)
Hepatic ceramides
LXR+/+ CTRL
LXR-/- CTRL
LXR+/+ FB1
LXR-/-FB1
Cer (d18:1/18:0)
Cer (d18:1/20:0)
T***, G***, TxG^ns
Cer (d18:1/26:0)
e
Hepatic sphingomyelins
d18:1 SM (ng / mg liver)
T***, G^ns, TxG^ns
T***, G*, TxG^ns
T***, G***, TxG^ns
T**, G**, TxG^ns
SM (d18:1/16:0)
SM (d18:1/22:0)
SM (d18:1/24:0)
SM (d18:1/24:1)
Hepatic sphingomyelins
T***, G^ns, TxG^ns
T^ns, G**, TxG^ns
T^ns, G^ns, TxG^ns
T**, G^ns, TxG^ns
T*, G^ns, TxG^ns
T***, G*, TxG^ns
SM (d18:1/16:1)
SM (d18:1/18:0)
SM (d18:1/18:1)
SM (d18:1/20:0)
SM (d18:1/20:1)
SM (d18:1/22:1)

Figure 3

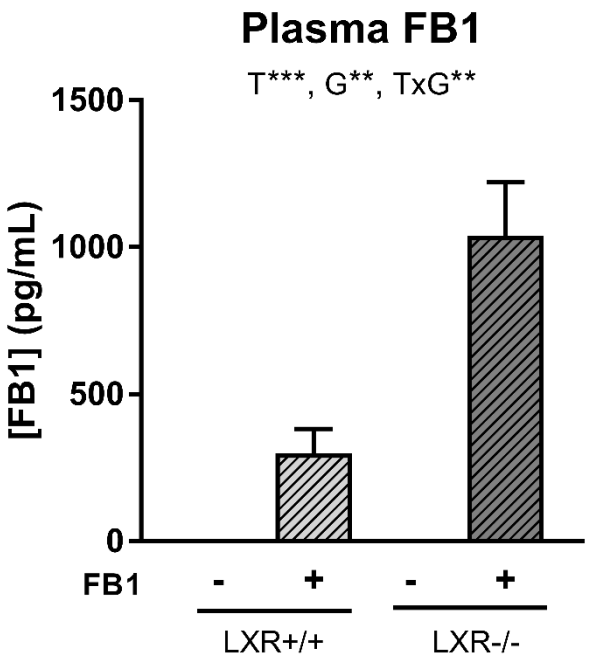

Figure 4

a

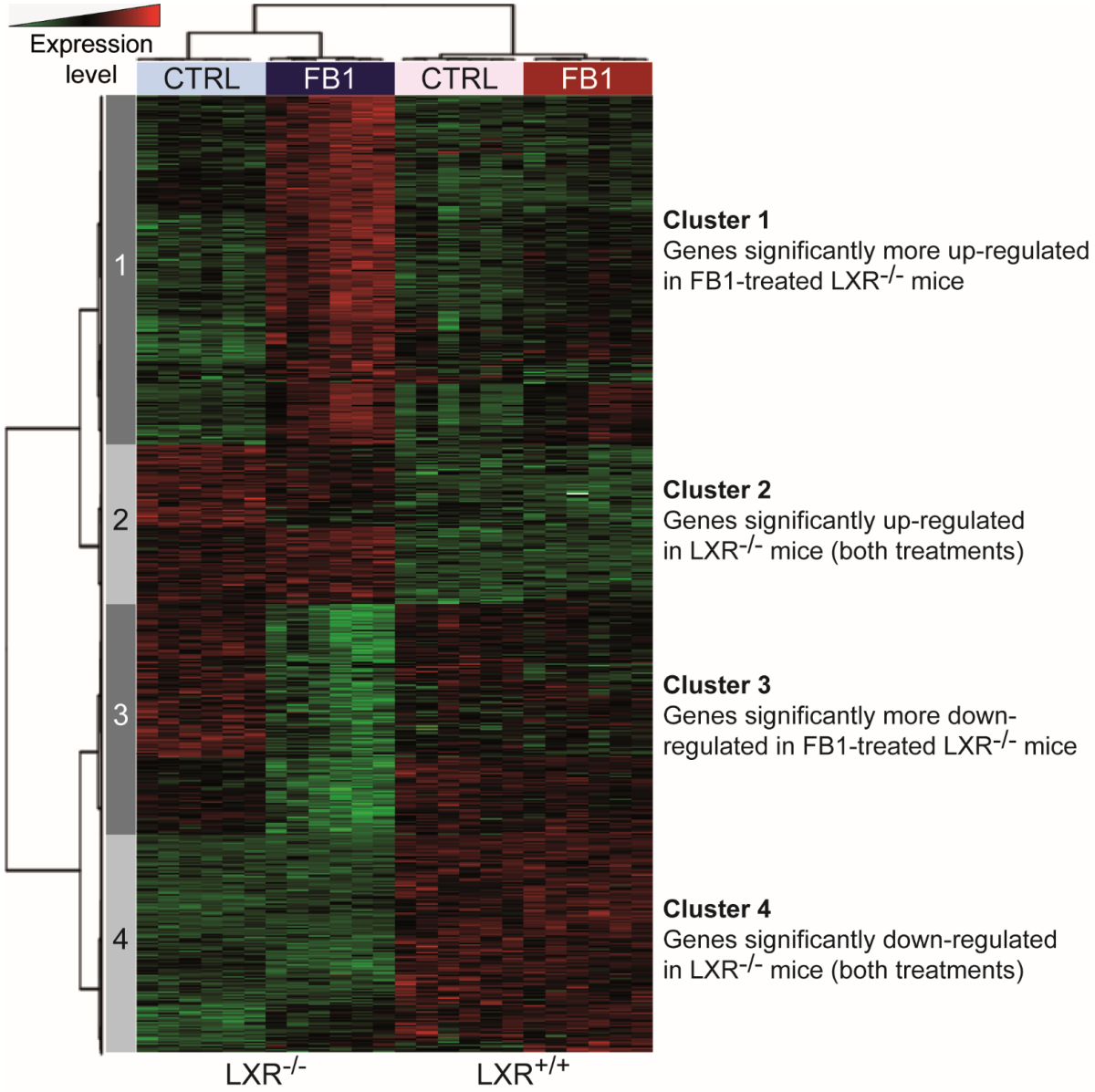

b

Cluster 1

- Focal adhesion
- PI3K-AKT signaling pathways
- Proteoglycans in cancers
- ECM-receptor interaction
- Chronic myeloid leukemia

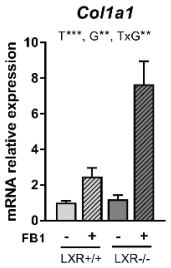

Cluster 2

- Cytokine receptors interaction
- Catalytic activity

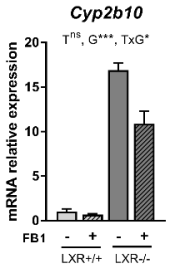

Cluster 3

- Metabolic pathways
- VAL, LEU and ILEU degradation
- ALA, ASP and GLUT metabolism
- Drug metabolism
- Bile secretion

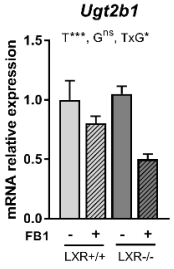

Cluster 4

- PPAR signaling pathway
- Pyruvate metabolism
- Fatty acid metabolism

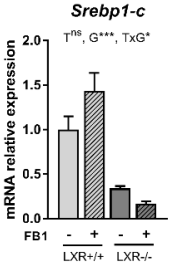

revised Figure 5

a

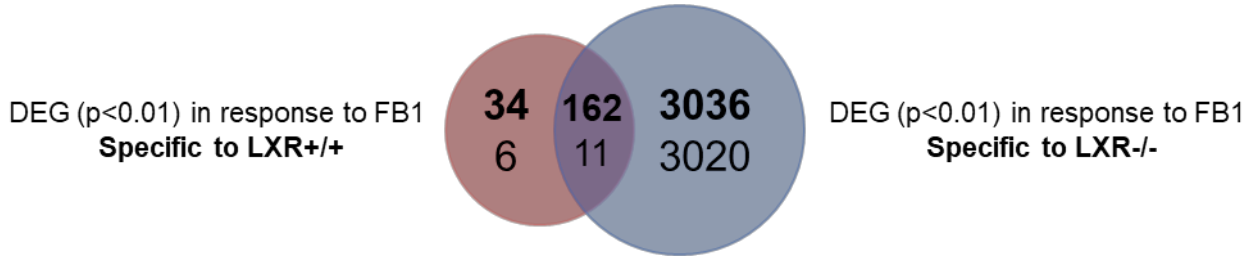

b

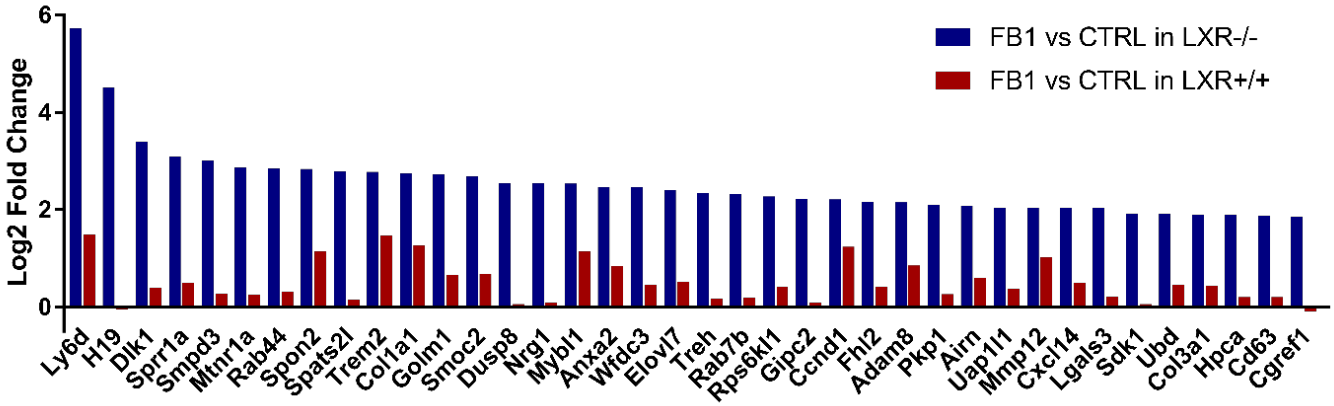

c

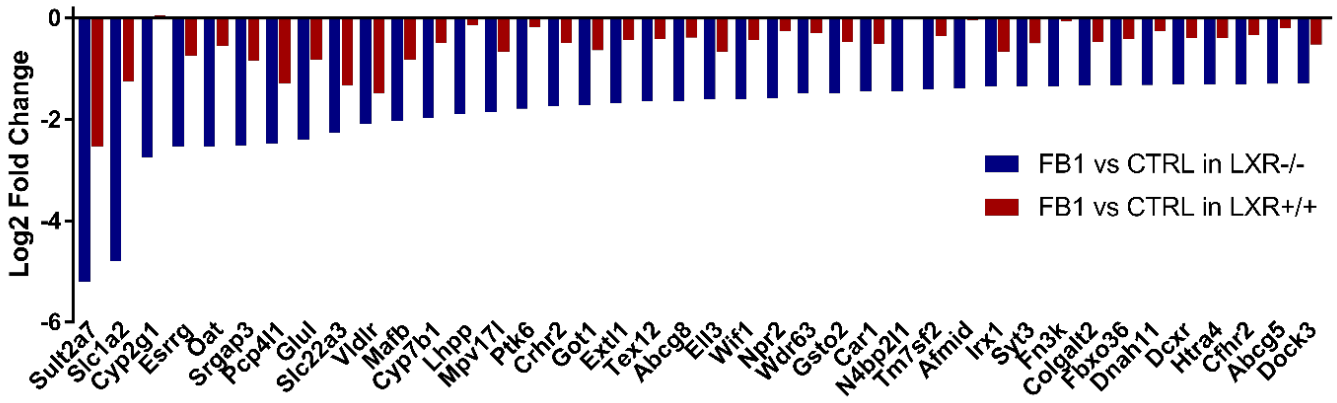

d

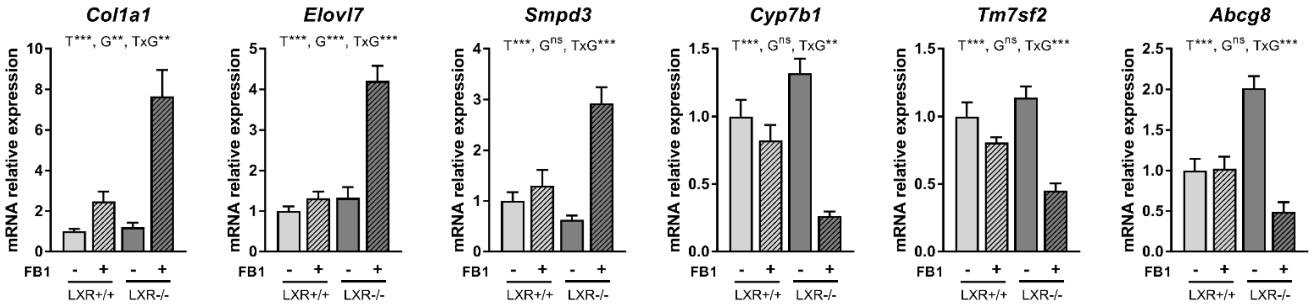

Figure 6

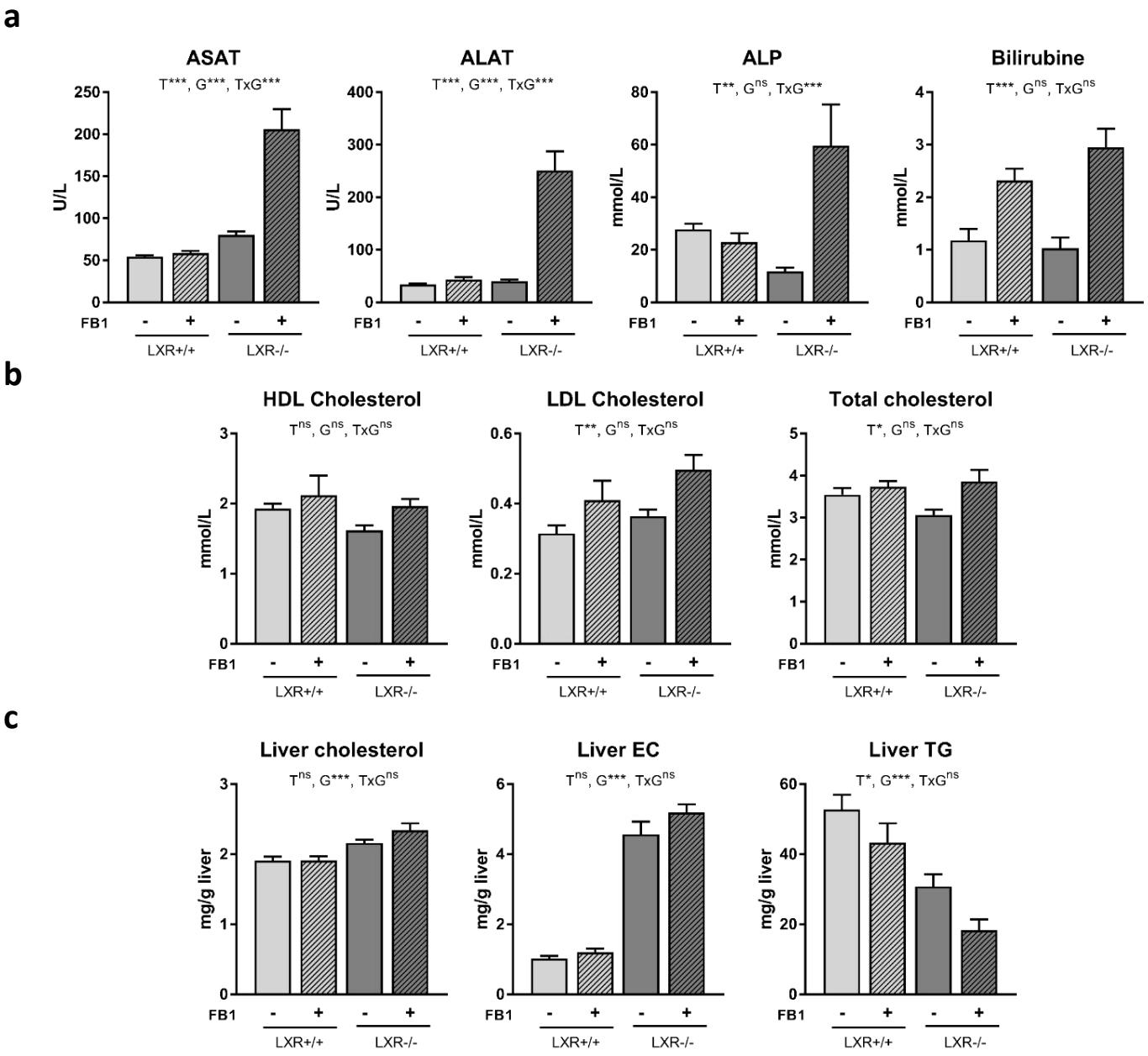
a
ASAT
T***, G***, TxG***
U/L
ALAT
T***, G***, TxG***
U/L
ALP
T**, G^ns, TxG***
mmol/L
Bilirubine
T***, G^ns, TxG^ns
mmol/L
FB1
LXR+/+
LXR-/-
b
HDL Cholesterol
T^ns, G^ns, TxG^ns
mmol/L
LDL Cholesterol
T**, G^ns, TxG^ns
mmol/L
Total cholesterol
T*, G^ns, TxG^ns
mmol/L
c
Liver cholesterol
T^ns, G***, TxG^ns
mg/g liver
Liver EC
T^ns, G***, TxG^ns
mg/g liver
Liver TG
T*, G***, TxG^ns
mg/g liver

Figure 7

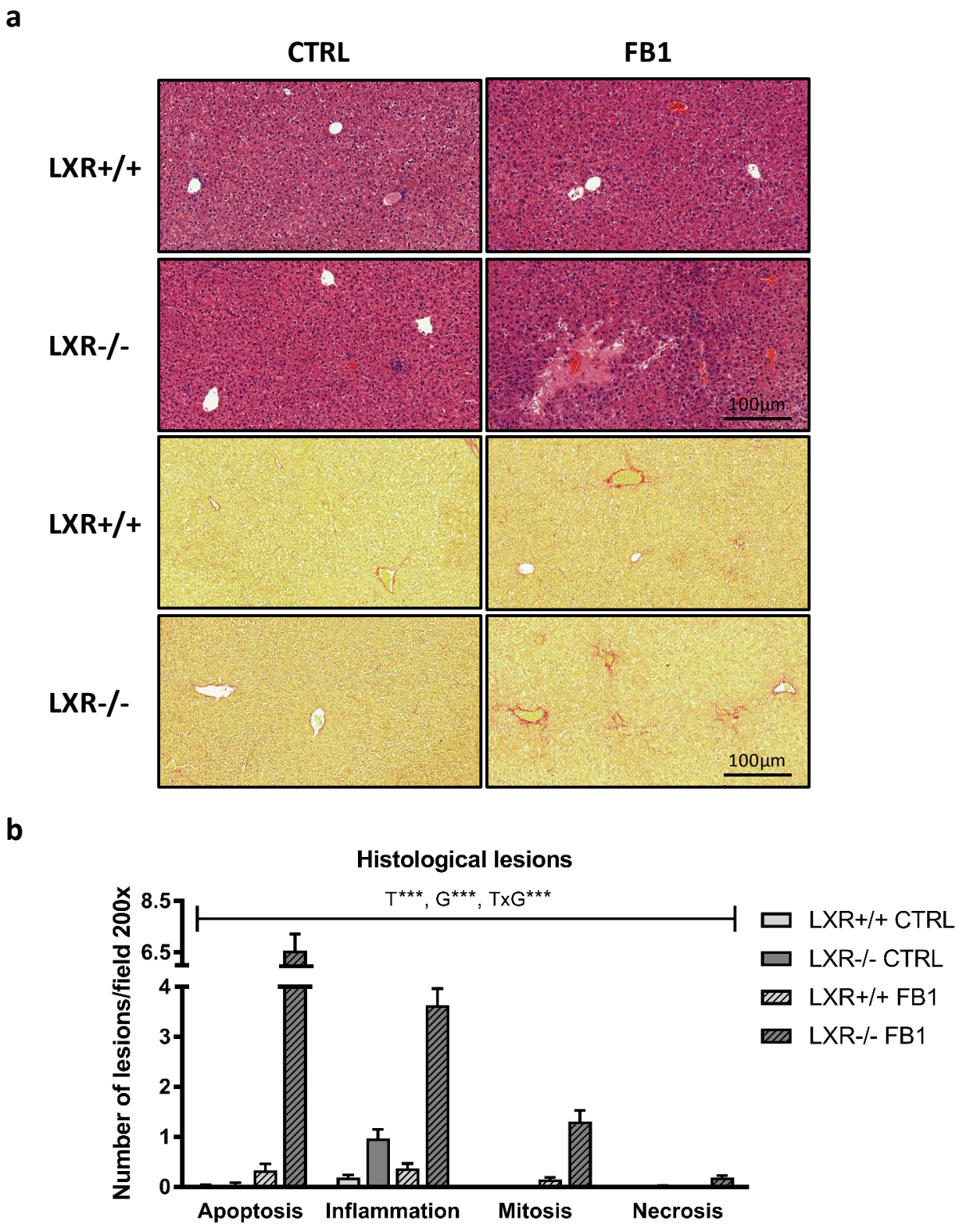
a
CTRL
FB1
LXR+/+
LXR-/-
LXR+/+
LXR-/-
100µm
100µm
b
Histological lesions
T***, G***, TxG***
Number of lesions/field 200x
8.5
6.5
4
3
2
1
0
Apoptosis
Inflammation
Mitosis
Necrosis
LXR+/+ CTRL
LXR-/- CTRL
LXR+/+ FB1
LXR-/- FB1

Online Resource 1: Oligonucleotide sequences for real-time PCR

Gene	NCBI Refseq	Forward primer (5'-3')	Reverse primer (5'-3')
Abcg8	NM_026180	ATCCATTGGCCACCCTTGT	GCGTCTGTCGATGCTGGTC
CerS2	NM_029789	CAGCTCTGCACCGGACG	GGTTAAGTTCACAGGCAGCCAT
Col1a1	NM_007742	GGCTCCTGCTCCTCTTAGGG	TCGGGTTTCCACGTCTCAC
Cyp2b10	NM_009999	TTTCTGCCCTTCTCAACAGGAA	ATGGACGTGAAGAAAAGGAACAAC
Cyp2e1	NM_000773	CTGTGTTCCAGGAGTACAAGAACAAG	TCCTTCCATGTGGGTCCATT
Cyp7b1	NM_007825	ACATGGTGACACTTTCACTGTCTTC	GAACTTCTGAAAGCTTAATTGTTTTGG
Elovl7	NM_029001	TCATGGAGAACCGGAAGCC	AATGTCACATCGAAACGAGTAACCT
Got1	NM_010324	TCCAGATCCCCGCAAGGT	CCTTCCTCACTACTGGCAAAACC
Psmb6	NM_008946	GGAAGTCTCCACAGGGACCA	AACCACGCCCCCATTAAACT
Smpd1	NM_011421	TGGTTACCAGCTGATGCCC	AGGCGGAGGCCAGGG
Smpd3	NM_018667	CCAATGGGTGCAGCTTCG	AACAATTCTTTGGTCCTGAGGTG
Srebp1-c	NM_011480	GGAGCCATGGATTGCACATT	GCTTCCAGAGAGGAGGCCAG
Tm7sf2	NM_028454	AAGGCCTGGAACTGAAGGACA	ACCAGAGCCTGGAAGCCAT
Ugt2b1	NM_152811	GTTTTCTCTGGGATCAATGGTTAAA	TTTCTTACCATCAAATCTCCACAGAAC

Online Resource 2: Pathways significantly up-regulated specifically in LXR$^{-/-}$ mice treated with FB1

Pathway description	Observed gene count	False discovery rate
Focal adhesion	33	5.04e-10
PI3K-Akt signaling pathway	41	9.61e-09
Proteoglycans in cancer	31	2.28e-08
ECM-receptor interaction	17	1.9e-06
Chronic myeloid leukemia	15	2.33e-06
Amoebiasis	19	4.27e-06
Osteoclast differentiation	19	6.32e-06
MicroRNAs in cancer	20	9.93e-06
Protein digestion and absorption	15	3.51e-05
Viral carcinogenesis	23	4.66e-05
Pathways in cancer	30	0.000117
HTLV-I infection	26	0.000217
Glioma	11	0.00024
Regulation of actin cytoskeleton	22	0.000402
p53 signaling pathway	11	0.000629
Cytokine-cytokine receptor interaction	23	0.00105
MAPK signaling pathway	23	0.00134
Hepatitis B	16	0.00161
Colorectal cancer	10	0.00164
Prostate cancer	12	0.00164
Chemokine signaling pathway	18	0.00173
Pancreatic cancer	10	0.00173
Endocytosis	20	0.00178
Endocytosis	8	0.00249
Melanoma	10	0.00284
Natural killer cell-mediated cytotoxicity	13	0.00369
Bacterial invasion of epithelial cells	10	0.00524
Thyroid cancer	6	0.00648
Transcriptional misregulation in cancer	15	0.00947
Thyroid hormone synthesis	9	0.0105
Platelet activation	13	0.0107
Vasopressin-regulated water reabsorption	7	0.0107
Small cell lung cancer	10	0.0116
Neurotrophin signaling pathway	12	0.0131
Dilated cardiomyopathy	10	0.0142
Ras signaling pathway	18	0.0148
Cell cycle	12	0.0152
Leukocyte transendothelial migration	12	0.0152
Bladder cancer	6	0.0152
Leishmaniasis	8	0.0192
Estrogen signaling pathway	10	0.0199
Phagosome	14	0.0216
Apoptosis	9	0.0225
Glutathione metabolism	7	0.0259
Hippo signaling pathway	13	0.027
Gap junction	9	0.0306
Thyroid hormone signaling pathway	11	0.0306
NF-kappa B signaling pathway	9	0.0389

Online Resource 3: Pathways significantly down-regulated specifically in LXR$^{-/-}$ mice treated with FB1 (p<0.01)

Pathway description	Observed gene count	False discovery rate
Metabolic pathways	83	3.84e-17
Valine, leucine, and isoleucine degradation	10	2.13e-05
Alanine, aspartate, and glutamate metabolism	8	0.000108
Arginine and proline metabolism	9	0.000305
Phenylalanine metabolism	6	0.000305
Glyoxylate and dicarboxylate metabolism	6	0.000767
Nitrogen metabolism	5	0.00118
Propanoate metabolism	6	0.00213
Drug metabolism - other enzymes	7	0.00377
Microbial metabolism in diverse environments	13	0.00377
Biosynthesis of amino acids	8	0.00693
Tyrosine metabolism	6	0.00716
Pyrimidine metabolism	9	0.00834
Tryptophan metabolism	6	0.00834
Selenocompound metabolism	4	0.00834
Pantothenate and CoA biosynthesis	4	0.00834
Peroxisome	8	0.00834
beta-Alanine metabolism	5	0.00915
Linoleic acid metabolism	6	0.00915
2-Oxocarboxylic acid metabolism	4	0.00915
Serotonergic synapse	10	0.0105
Glycerophospholipid metabolism	8	0.013
Bile secretion	7	0.0151
Glycine, serine, and threonine metabolism	5	0.0212
Carbon metabolism	8	0.0345